www.czasopisma.pan.pl PAN www.journals.pan.pl

ARCHIVES of FOUNDRY ENGINEERING

VERSITA

DOI: 10.2478/v10266-012-0100-3

ISSN (2299-2944)
Volume 12
Issue 4/2012

Published quarterly as the organ of the Foundry Commission of the Polish Academy of Sciences

11 – 16

Modelling of Eutectic Saturation Influence on Microstructure in Thin Wall Ductile Iron Casting Using Cellular Automata

A.A. Burbelko*, D. Gurgul, W. Kapturkiewicz, M. Górny
AGH University of Science and Technology, 23 Reymonta Str., Krakow, Poland
*Corresponding author. E-mail address: abur@agh.edu.pl

Received 02.06.2012; accepted in revised form 03.09.2012

Abstract

The mathematical model of the globular eutectic solidification in 2D was designed. Proposed model is based on the Cellular Automaton Finite Differences (CA-FD) calculation method. Model has been used for studies of the primary austenite and of globular eutectic grains growth during the ductile iron solidification in the thin wall casting. Model takes into account, among other things, non-uniform temperature distribution in the casting wall cross-section, kinetics of the austenite and graphite grains nucleation, and non-equilibrium nature of the interphase boundary migration. Calculation of eutectic saturation influence (S_c = 0.9 - 1.1) on microstructure (austenite and graphite fraction, density of austenite and graphite grains) and temperature curves in 2 mm wall ductile iron casting has been done.

Keywords: Solidification Process, Thin Cellular Automaton, Modelling

1. Introduction

Nodular graphite cast iron, also known as ductile iron (DI), has major applications in critical engineering parts due to its mechanical properties and castability. The mechanical and physical properties of this material depend on the shape and number of the graphite grains and microstructure of the metallic matrix.

Solidification of DI was a subject of many computer modelling programs described in literature [1-5], in which the stationary conditions of carbon diffusion in austenite is pre-assumed. Recently, a tendency for production of thin-walled castings has been observed [6-8]. In this technology, the process of the fast solidification may be very far from equilibrium and steady-state conditions [9].

The purpose of the present work is a two-dimension model development for simulation of the DI structure formation during the solidification in the condition of non steady-state temperature and diffusion fields in the thin-wall casting.

2. Model of process

The CA-FD is one of the known methods of the simulation of microstructure formation during the solidification [10, 11]. In the CA microstructure modelling the outer grain shape is the result of the simulation and does not superimposed beforehand. The model development for a one-phase microstructure evolution is a subject of the numerous researches [12-21]. Model of the eutectic solidification of DI in the uniform temperature field and superimposed cooling rate is known [22].

Presented model is based on the CA-FD technique and will predict solidification of DI in the non-uniform temperature field during the cooling of the thin-wall casting in the sand mould. Model takes into account the continuous nucleation of austenite

and graphite grains from liquid controlled by undercooling, separate non-equilibrium growth of graphite nodules and austenite dendrites at the first solidification stage, and the following cooperative growth of graphite-austenite eutectic in the binary Fe-C system. A set of six cell states for microstructure modelling: three mono-phase states – "liquid", "austenite", and "graphite" – and three two-phase states were used.

At the beginning, all of the cells in the CA lattice are in the "liquid" state and have initial temperature. The analysed casting domain is in the thermal contact with a sand mould with a normal initial temperature. Nucleation and growth of the solid grains are possible when the temperature of the liquid drops below the liquidus.

2.1. Heat and mass diffusion

The numerical solution of the nonlinear Fourier equation was used for heat flow in the analyzed domains (casting and mould):

$$c\frac{\partial T}{\partial \tau} = \nabla(\lambda \nabla T) + q_T \tag{1}$$

where: T is the temperature, τ is the time, λ is the thermal conductivity, and c is the volumetric specific heat, q_T is the latent heat generation rate.

Solute diffusion in the domains of every phase was calculated in the same manner as temperature distribution, by the numerical solution of the diffusion equation with a source term at the interface:

$$\frac{\partial C}{\partial \tau} = \nabla(D \nabla C) + q_C \tag{2}$$

where D is the solute diffusion coefficient, and C is the solute concentration in this phase.

Both source functions are equal to zero outside of the interface cells. In the interface cells the value of the heat and mass sources for the finite-difference scheme are:

$$q_T = L_{\alpha\to\beta}\frac{\partial f_\beta}{\partial \tau} \tag{3}$$

$$q_C = (C_\alpha - C_\beta)\frac{\partial f_\beta}{\partial \tau} \tag{4}$$

where $L_{\alpha\to\beta}$ is the volumetric latent heat of $\alpha\to\beta$ transformation, C_α and C_β are the carbon concentrations in the vanishing and growing phases, and Δf_β is the growth of the new phase volume fraction during the time step.

For thermal and diffusion calculation in the casting region, the following boundary conditions were used: at the top and bottom of the grid – periodic boundary condition; at the left side – symmetry BC; at the right side – mould with an absence of mass flow and heat flow through the border according to Newton law:

$$q = h(T_c - T_m) \tag{5}$$

where h is the heat transfer coefficient (value of 500 $W \cdot m^{-2}K^{-1}$ was assumed), and T_c and T_m are the temperature values of the casting and mould surfaces in the contact.

The details of solution are described in [23].

2.2. Nucleation

According to [24] undercooling of the nucleation from liquid during ductile iron solidification in the thin wall reaches up to 65 K below the equilibrium temperature. Grain nucleation in industrial alloys has a heterogeneous nature. The substrates for the nucleus are randomly distributed in the bulk. Bulk distribution of differently-sized substrates also has a stochastic nature. The undercooling value of substrate activation is a function of its size. Functional relationship between the active substrate fraction and undercooling ΔT should be a feature of the probability distribution law [25]. The undercooling value of each phase should be calculated relative to the appropriate liquidus lines.

The number of active substrates in the domain V of the melt with an undercooling ΔT below the liquidus may be calculated on the basis of the cumulative distribution function $F(\Delta T)$:

$$N = N_{\max} F(\Delta T) V \tag{6}$$

where: N_{max} is the maximum specific number of substrates for nucleation.

When one substrate position doesn't have any influence on another substrate's positions, the random variable calculated as the number of substrates in any random domain V will have the Poisson statistical distribution with the mean value $\nu = N_{max}V$. For this statistical distribution the probability density function is

$$P_r(k) = e^{-\nu}\nu^k / k! \tag{7}$$

where: e is the Euler-Mascheroni constant, and k is the estimated number of substrates.

The method of nucleation modelling for a CA lattice is known [25]. According to [25] the undercooling values randomly generated with a statistical distribution curve are attributed to randomly chosen cells. If a cell is chosen several times (i.e., if it contains more than one nucleation site), only the smaller nucleation undercooling is used. If the CA cell is too high/large in size, the calculated grain density will be underestimated. A modified version of this algorithm was used in this paper.

The probability of the lack of a nucleus in the cell ($k = 0$) according to Poisson's statistic is equal to:

$$P_r(k=0) = e^{-\nu} \tag{8}$$

The probability of one substrate ($k = 1$) in the cell is represented by the following equation:

$$P_r(k=1) = \nu e^{-\nu} \tag{9}$$

The probability of more than one substrates in one cell may be calculated as:

$$P_r(k>1) = 1 - \nu e^{-\nu}(1+\nu) \tag{10}$$

The next way of substrate placement and the undercooling of nucleation selection is proposed based on the mean number of active substrates in one cell:

$$\nu = N_{max} F(\Delta T)\upsilon \tag{11}$$

where υ is a cell's volume (or surface for 2D).

For each of the cells in the CA a random number p should be generated with an equiprobability distribution in the (0..1] range. For small domains when $\nu << 1$ this value is equal to probability of one substrate presence in the analyzed domain. Because for small cells $P_r(k=0 \text{ or } k=1) \to 1$ and $P_r(k>1) \to 0$, the condition of the precise one substrate present in the cell is the following inequality:

$$p < N_{max} F(\Delta T)\upsilon \tag{12}$$

The nucleation undercooling in this case should be estimated on the basis of the inverse function of the above-mentioned cumulative distribution curve (fractile):

$$\Delta T = F^{-1}\left[p(\upsilon N_{\max})^{-1}\right] \tag{13}$$

The solid grain will begin to grow when the undercooling exceeds the above level. The substrates are present (and nucleation is possible) only in cells with a positive ΔT value.

The method of continuous nucleation prediction used in modelling has been presented in details in the [26].

The Weibull statistical distribution was used in this paper for nucleation modelling [27]. The specific number of active substrates is given by:

$$n = N_{\max} \exp\left(-b \cdot \Delta T^{-1}\right) \tag{14}$$

where N_{max} and b is a nucleation parameters.

The undercooling of nucleation can be calculated as

$$\Delta T = -b\left\{\ln\left[p\,(\upsilon N_{\max})^{-1}\right]\right\}^{-1} \tag{15}$$

where p is a random number generated with an equiprobability distribution in the (0..1] range.

The values for N_{max} and b used in the present work for the modelling of graphite and austenite grains nucleation are listed in the table 1. The solid grain will begin to grow when the undercooling exceeds the above level. The substrates are present (and nucleation is possible) only in cells with a positive ΔT value. The state of the CA cell with the active nucleus varies from "liquid" to "austenite" or "graphite". The states of adjacent liquid cells are changed to the appropriate interface. The new phase growth and volume fraction changes are only possible in the interface cells.

Table 1.
Nucleation parameters

	Austenite	Graphite
b (K)	5	50
N_{max} (m^{-2})	$3 \cdot 10^8$	$1 \cdot 10^9$

2.3. Grain growth

The kinetic undercooling of the mother liquid phase is a thermodynamic driving force of the new grains' growth. Total undercooling at the solid-liquid interface, hence the difference between the equilibrium solidification temperature T_{Eq} (determined from the phase equilibrium diagram of carbon concentration obtained during simulation on the transformation front) and the real temperature T_r is equal to the sum of capillary undercooling ΔT_κ and kinetic undercooling ΔT_μ:

$$T_{Eq} - T_r = \Delta T_\kappa + \Delta T_\mu \tag{16}$$

where $\Delta T_\kappa = \Gamma\kappa$, Γ is the Gibbs-Thomson coefficient, and κ is a front curvature.

Basing on [28], it has been assumed in the computations that the interface migration rate u is a linear function of the local kinetic undercooling ΔT_μ:

$$u = \mu \Delta T_\mu \tag{17}$$

where μ is the kinetic growth coefficient.

The increment of the new phase volume fraction in the interface cells Δf over one time step $\Delta\tau$ in the square CA cells of size a was calculated using the equation proposed in [29]:

$$\Delta f = u\,\Delta\tau \cdot \left[a(|\cos\theta| + |\sin\theta|)\right]^{-1} \tag{18}$$

where θ is the angle between the X axis and the normal direction of the grain interface.

If the phase volume fraction in the interface cell increases up to 1, this cell varies they state from interface to appropriate one-phase. Additionally, this cell captures all of the adjacent ones: their states exchange to the appropriative interface.

The normal direction of the grain boundary in the interface cells was determined by the approach of the F-vector [30]. The angle θ between the growth direction (normal to the grain boundary) and the positive X-axis direction was calculated as follows:

$$\theta = \arctan\left[\sum_{i,j} y_{i,j} f_{i,j} \cdot \left(\sum_{i,j} x_{i,j} f_{i,j}\right)^{-1}\right] \tag{19}$$

where: $f_{i,j}$ is the volume fraction of the phase in the cell (i,j), and $x_{i,j}$ and $y_{i,j}$ are the relative coordinates of the adjacent cells. The summation in (19) concerning the 20 neighbouring cells gives the best results of normal direction estimation [29].

Another details of the used CA-FD model of a two-phase eutectic solidification were introduced elsewhere [31, 32].

3. Parameters for modelling

Computations of the diffusion field and microstructure were carried out on a grid of 250×1000 cells. The side of each cell was 1 μm in length. An initial uniform carbon concentration in the binary Fe-C liquid for five alloys with the different eutectic equivalent used in the simulation are shown in the Table 2.

Table 2.

Eutectic Saturation, S_c	Carbon concentration, % mas.	Initial temperature, °C
0.90	3.83	1254.9
0.95	4.04	1228.9
1.00	4.25	1203.0
1.05	4.46	1283.5
1.10	4.68	1364.0

Equal initial superheating equal to 50 K was assumed (above the austenite liquidus for hypoeutectic iron and above the graphite liquidus for hypereutectic one).

Parameters used in the modelling are shown in the Table 3.

Table 3.
Thermo-physical parameters used in the modelling.

Heat conductivity ($W \cdot m^{-1} \cdot K^{-1}$):			
– liquid	λ_L	30	[16]
– austenite	λ_γ	20	[33]
– graphite	λ_{gr}	20	[16]
– mould	λ_m	0,65	
Diffusivity of carbon in (m^2/s):			
– liquid	D_L	$1.25 \cdot 10^{-9}$	[34]
– austenite	D_γ	$5 \cdot 10^{-10}$	[16]
Transition heat (J/m^3):			
– liquid – austenite	$L_{L/\gamma}$	$19.7 \cdot 10^8$	[33]
– liquid – graphite	$L_{L/gr}$	$16.2 \cdot 10^5$	
– austenite – graphite	$L_{\gamma/gr}$	$8.8 \cdot 10^5$	
Specific heat ($J \cdot m^{-3} \cdot K^{-1}$):			
– liquid	$c_{v,L}$	$5.6 \cdot 10^6$	[33]
– austenite	$c_{v,\gamma}$	$5.84 \cdot 10^6$	[16]
– graphite	$c_{v,gr}$	$1.78 \cdot 10^6$	[33]
– mould	c_m	$1.67 \cdot 10^6$	
Gibbs-Thomson coefficient for interface ($m \cdot K$):			
– austenite – liquid	$\Gamma_{\gamma/L}$	$1.9 \cdot 10^{-7}$	[33]
– graphite – liquid	$\Gamma_{gr/L}$	$7.0 \cdot 10^{-6}$	
– graphite – austenite	$\Gamma_{gr/\gamma}$	$9.45 \cdot 10^{-6}$	
Kinetic coefficient of the interface ($m \cdot s^{-1} \cdot K^{-1}$):			
– austenite – liquid	$\mu_{\gamma/L}$	10^{-3}	[35]
– graphite – liquid	$\mu_{gr/L}$	10^{-8}	
– graphite – austenite	$\mu_{gr/\gamma}$	10^{-8}	

On the long sides of this mesh the periodic boundary condition (BC) was used [36] and on the short sides of this mesh the adiabatic one was used. For the temperature field simulation the following BC were using: the periodic BC for long sides, the adiabatic one at the casting axis (left side in the figure 1) and Newton BC with heat transfer coefficient h = 500 $W \cdot m^{-2} \cdot K^{-1}$ between casting and mould (right side in figure 1).

Casting is cooled in the green sound mould. For the temperature field calculation in the casting the 5× 20 "rare" mesh was used with the spatial step equal to 50 μm. Mould initial temperature was equal to T_m = 298 K. On the long sides of this mesh the periodic BC was used. On the short outer side the Newton BC was assumed with h = 100 $W \cdot m^{-2} \cdot K^{-1}$.

Simulation for every chemical compositions of the DI has been repeated five times.

4. Results of modelling

The example of the history of microstructure formation in the 2 mm casting is presented in Figure 1 for eutectic DI.

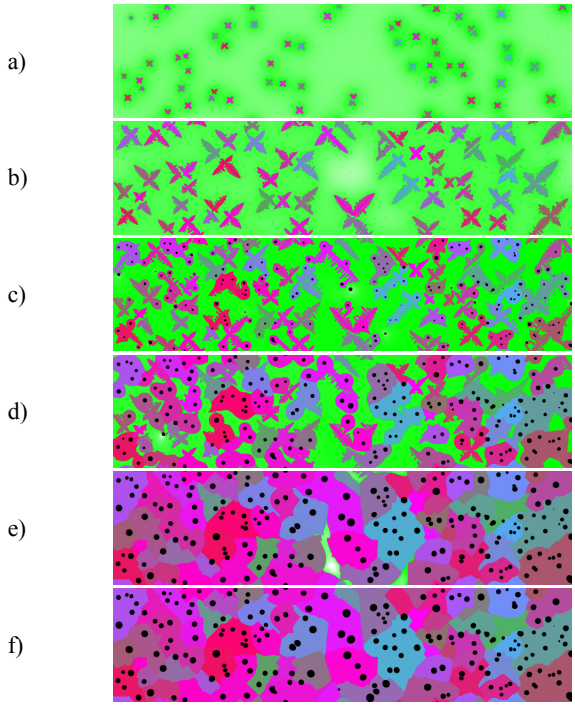

Fig. 1. Microstructure of the eutectic DI (simulation results); cooling time, s: a) 1.2, b) 3.0, c) 5.2; d) 7.7; e) 13.3; f) 15.9

The comparison of the virtual microstructure and microstructure of the real 2 mm casting (non-etched) is shown respectively in figures 2a and 2b for hypereutectic DI (S_c = 1.1). The simulated graphite nodules size and bulk distribution are similar to the experimental one.

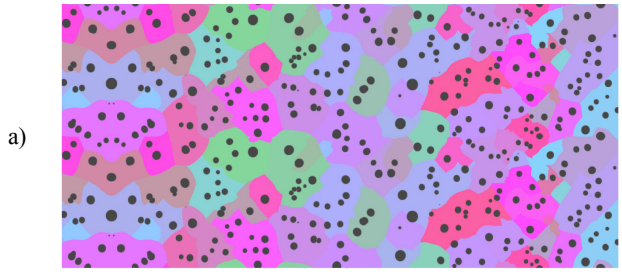

b)

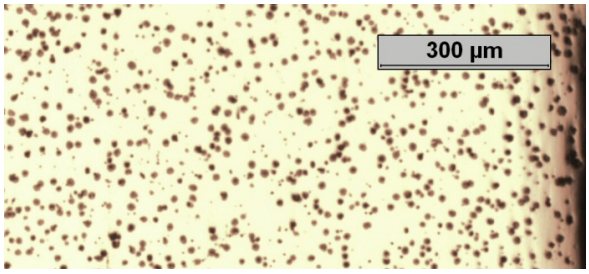

← *casting centre* *mould wall* →

Fig. 2. Final microstructure of the DI in the 2 mm wall: a) simulation for S_C = 1.1, separate austenite grains have different colour (results of modelling are repeated 4 times due to symmetry and periodic boundary conditions); b) real casting, DI with S_C = 1.1 (un-etched).

Volume fraction of solidified austenite, similarly as volume fraction of graphite depends linearly on eutectic saturation. The averaged results of simulations are shown in the Figure 3 with the 90% confident limits.

The important factor for casting quality is density of grains. In Figure 4 is visible, that the maximum the grain density of the casting (number of grains on surface area) is placed near the eutectic composition (S_c = 1.0...1.05).

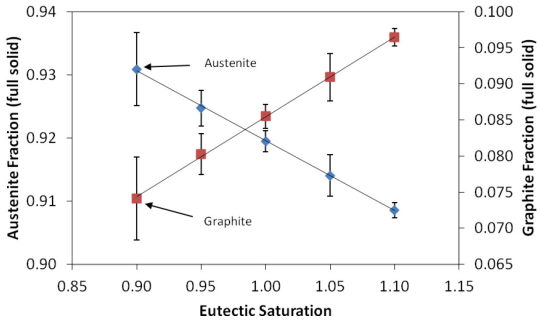

Fig. 3. Influence of eutectic saturation S_c on the austenite and graphite volume fraction

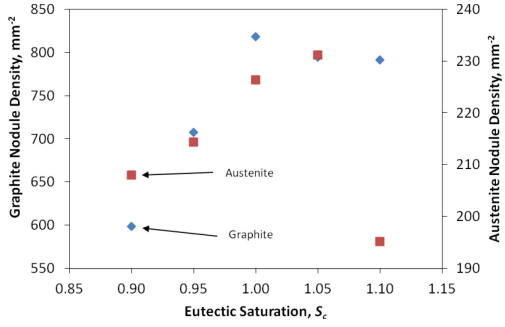

Fig. 4. Influence of eutectic saturation Sc on austenite and graphite grain density

We assume that for all cases of S_c is the same overheating, so, in this case were different start (pouring) temperatures and different shapes of cooling curves – Fig. 5 and Table 3 – as the result – diversity in structures (Fig. 3 and 4).

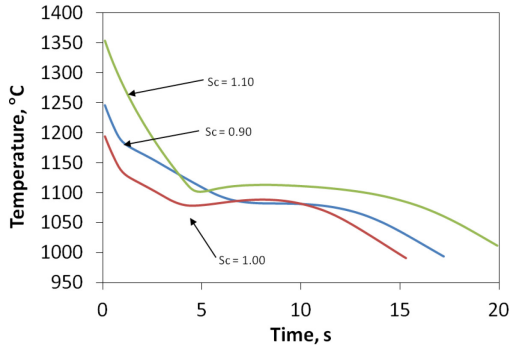

Fig. 5. Average cooling curves for S_c = 0.90, 1.00, 1.10

5. Conclusions

The CA-FD computer model for the simulation of the DI solidification in thin wall was presented. The results of modelling were compared with the experimental microstructure. Results obtained in the 2 mm width casting wall confirm the model accuracy.

The model is well worked for thin walled ductile iron casting when the solidification process is very fast.

Volume fraction of solidified austenite, similarly as volume fraction of graphite depends linearly on eutectic saturation. The maximum the grain density (number of grains on surface area) is placed near the eutectic saturation (S_c = 1.0).

Acknowledgements

This work was supported by Polish NCN project No. N N508 621140.

References

[1] Stefanescu, D.M., Catalina, A., Guo, X., Chuzhoy, L, Pershing, M.A. & Biltgen, G.L. (1998). Prediction of room temperature mcrostructure and mechanical properties in iron castings. In VIII Scientific International Conference Modeling of Casting, Welding and Advanced Solidification Processes, June 7-12, 1998 (pp. 455–462). San Diego, CA, ed. B.G. Thomas & C. Beckermann: TMS, Warrendale.

[2] Yoo, S.M., Ludwig, A. & Sahm, P.R. (1997). Numerical simulation of solidification of nodular cast iron in permanent molds. In Proc. of the 4th decennial Intern. Conf. on Solidification Processing, 07-10. July, 1997 (pp. 494–497). Sheffield, UK, ed. J. Beech & H. Jones: Ranmoor House, Univ. of Sheffield.

[3] Chang, S., Shangguan, D. & Stefanescu, D. (1992). Modeling of the Liquid/Solid and the Eutectoid Phase Transformations in Spheroidal Graphite Cast Iron. *Metal. Trans. A*. 23A, 1333–1346.

[4] Skaland, T., Grong, O. & Grong, T. (1993). A Model for the Graphite Formation in Ductile Cast Iron. II. Solid State Transformation Reactions. *Metal. Trans. A.* 24A, 2347–2353.

[5] Onsoien, M., Grong, O., Gundersen, O. & Skaland, T. (1999). A process model for the microstructure evolution in ductile cast iron. I. The model. *Mat. Trans. A.* 30A, 1053–1068.

[6] Fraś, E. & Górny, M. (2011). Thin wall ductile and austempered iron castings as substitutes for aluminium alloy castings. *Foundry Trade J. Int.* 185, 85–90.

[7] Labrecque, C. & Gagne, M. (2003). Production of thin-wall ductile iron castings. *Int. J. of Cast Metals Res.* 16, 313–318.

[8] Stefanescu, D. M., Ruxanda, R. E. & Dix, L.P. (2003). The metallurgy and tensile mechanical properties of thin wall spheroidal graphite irons. *Int. J. of Cast Metals Res.* 16, 319–324.

[9] Fredriksson, H., Stjerndahl, J. & Tinoco, J. (2005). *Mat. Sci. Eng. A*. 413, 363.

[10] Rafii-Tabar, H. & Chirazi, A. (2002) Multiscale computational modelling of solidification phenomena. *Physics Reports Review Section of Physics Letters.* 365, 145–249.

[11] Lee, P. D., Chirazi, A., Atwood, R. C. & Wang, W. (2004). Multiscale modelling of solidification microstructures, including microsegregation and microporosity, in an Al-Si-Cu alloy. *Mat. Sci. Eng. A*. 365, 57–65.

[12] Umantsev, A. R., Vinogradov, V. V. & Borisov, V. T. (1985). Mathematical modeling of the dendrite growth during the solidification from undercooled melt. *Kristallografia.* 30, 455–60, (in Russian).

[13] Rappaz, M. & Gandin, Ch. A. (1993). Probabilistic Modelling of Microstructure Formation in Solidification Processes. *Acta Met. et Mater.* 41, 345–60.

[14] Pan, S. & Zhu, M. (2010). A three-dimensional sharp interface model for the quantitative simulation of solutal dendritic growth. *Acta Mater.* 58, 340–52.

[15] Guillemot, G., Gandin, Ch. A. & Bellet, M. (2007). Interaction between single grain solidification and macrosegregation: Application of a cellular automaton-Finite element model. *J. of Crystal Growth.* 303, 58–68.

[16] Beltran-Sanchez, L. & Stefanescu, D. M. (2004). A Quantitative Dendrite Growth Model and Analysis of Stability Concepts. *Metall. Mat. Trans. A.* 35, 2471–2485.

[17] Pavlyk, V. & Dilthey, U. (2004). Simulation of weld solidification microstructure and its coupling to the macroscopic heat and fluid flow modelling. *Modelling and Simulation in Mat. Science and Engineering*. 12, 33–45.

[18] Zhu, M. F. & Hong, C. P. (2002). A three dimensional modified cellular automaton model for the prediction of solidification microstructures. *ISIJ Int.* 42, 520–526.

[19] Jarvis, D. J., Brown, S. G. R. & Spittle, J. A. (2000). Modelling of non-equilibrium solidification in ternary alloys: comparison of 1D, 2D, and 3D cellular automaton-finite difference simulations. *Mat. Sci. Techn.* 16, 1420–4.

[20] Burbelko, A. A., Fraś, E., Kapturkiewicz, W. & Gurgul, D. (2010). Modelling of Dendritic Growth During Unidirectional Solidification by the Method of Cellular Automata. *Mat. Sci. Forum.* 649, 217–222.

[21] Burbelko, A. A., Fraś, E., Kapturkiewicz, W. & Olejnik, E. (2006). Nonequilibrium Kinetics of Phase Boundary Movement in Cellular Automaton Modelling. *Mat. Sci. Forum.* 508, 405–410.

[22] Zhao, H.L., Zhu, M. F. & Stefanescu, D. M. (2011). Modeling of the Divorced Eutectic Solidification of Spheroidal Graphite Cast Iron. *Key Eng. Materials.* 457, 324–329.

[23] Kapturkiewicz, W., Burbelko, A. A., Fraś, E., Górny, M. & Gurgul D. (2010). Computer modelling of ductile iron solidification using FDM and CA methods. *J. of Achievments in Materials and Manufacturing Engineering.* 43, 310–323.

[24] Górny, M. (2010) Solidification of thin wall ductile iron castings with hypereutectic composition. *ISIJ International* 50, 847-853.

[25] Gandin, Ch. A. & Rappaz, M. (1994). A Coupled Finite Element-Cellular Automaton Model for The Prediction Of Dendritic Grain Structures in Solidification Processes. *Acta Metall. Mater.* 42, 2233–2246.

[26] Burbelko, A., Fraś, E., Gurgul, D., Kapturkiewicz, W. & Sikora, J. (2011). Simulation of the Ductile Iron Solidification Using a Cellular Automaton. *Key Eng. Materials* 457, 330–336.

[27] Fraś, E., Wiencek, K., Burbelko, A.A. & Górny, M. (2006). The Application of Some Probability Density Function of Heterogeneous Nucleation. *Mat. Sci Forum* 508, 425–430.

[28] Hoyt, J. & Asta, M. (2002). Atomistic computation of liquid diffusivity, solid-liquid interfacial free energy, and kinetic coefficient in Au and Ag. *Phys. Rev.* B 65, 1–11.

[29] Burbelko, A.A, Kapturkiewicz, W. & Gurgul, D. (2007). Analysis of causes and means to reduce artificial anisotropy in modelling of the solidification process on cellular automaton. In Proc. of the 4th decennial Intern. Conf. on Solidif. Processing (Sheffield, UK, 07-10 July, 2007) ed J Beech and H Jones, 31–35.

[30] Dilthley, U. & Pavlik, V. (1998). Numerical simulation of dendrite morphology and grain growth with modified cellular automata. Modeling of Casting, Welding and Advanced Solidification Proc. VIII (San Diego, CA, June 7-12, 1998) ed. Thomas B. G. & Beckermann C. 589–596.

[31] Burbelko, A. & Gurgul, D. (2011). Modeling of primary and eutectic solidification by using CAFD method. *Computer Methods in Materials Science.* 11, 128–34.

[32] Gurgul, D. Burbelko, A. A. (2010). Simulation of austenite and graphite growth in ductile iron by means of cellular automata. *Archives of Metallurgy and Materials.* 55, 53–60.

[33] Kikoin, I.K. (1976). *Tablicy fiziczeskih velichin.* Moskwa Avtomizdat. (in Russian).

[34] Magnin, P., Mason, J. T. & Trivedi, R. (1991). Growth of Irregular Eutectic and the Al-Si System. *Acta Met. et Mater.* 39, 469–80.

[35] Burbelko, A. (2004). *Mezomodelowanie krystalizacji metodą automatu komórkowego*. Kraków, UWND AGH.

[36] Chopard, B. & Droz, M. (2005*). Cellular Automata Modeling of Physical Systems.* Cambridge University Press.